Tackling Oxygen Optode Drift: Near-Surface and In-Air Oxygen Optode Measurements on a Float Provide an Accurate in Situ Reference

HENRY C. BITTIG AND ARNE KÖRTZINGER

Marine Biogeochemistry Department, GEOMAR Helmholtz Centre for Ocean Research Kiel, Kiel, Germany

ABSTRACT

A yet unexplained drift of (some) oxygen optodes during storage/transport and thus significant deviations from factory/laboratory calibrations have been a major handicap for autonomous oxygen observations. Optode drift appears to be systematic and is predominantly a slope effect due to reduced oxygen sensitivity. A small contribution comes from a reduced luminophore lifetime, which causes a small positive offset. A reliable in situ reference is essential to correct such a drift. Traditionally, this called for a ship-based reference cast, which poses some challenges for opportunistic float deployments. This study presents an easily implemented alternative using near-surface/in-air measurements of an Aanderaa optode on a 10-cm stalk and compares it to the more traditional approaches (factory, laboratory, and in situ deployment calibration). In-air samples show a systematic bias depending on the water saturation, which is likely caused by occasional submersions of the standard-height stalk optode. Linear regression of measured in-air supersaturation against in-water supersaturation (using ancillary meteorological data to define the saturation level) robustly removes this bias and thus provides a precise (0.2%) and accurate (1%) in situ correction that is available throughout the entire instrument's lifetime.

1. Introduction

The use of optode in-air measurements as a potential reference has been suggested with the advent of optical oxygen sensors on floats (Körtzinger et al. 2005). This, however, received little further attention due to the optical technology's promise to be long-term stable. Despite proven in situ stability (e.g., Tengberg et al. 2006; Takeshita et al. 2013), it became evident in recent years that a drift occurs frequently, mostly during periods when sensors were not deployed in the field (Bittig et al. 2012; Takeshita et al. 2013; D'Asaro and McNeil 2013), and in situ calibration has become a crucial part.

In situ calibration can be done using Winkler-type oxygen titration of discrete samples from a hydrocast taken at the time and place of the float deployment (requires adequate ship capabilities and gives only information at the beginning; see section 2d), through comparison to an oxygen climatology (relying on a smoothed, potentially coarse set of historical data; see Takeshita et al. 2013), or by comparing in-air optode measurements with an atmospheric pO_2 (continuous throughout deployment, albeit only at one O_2 level). In-air referencing thus appeared on the agenda again and Fiedler et al. (2013) demonstrated the principle's feasibility, while Emerson and Bushinsky (2014) and S. Bushinsky et al. (2015, unpublished manuscript) show that such measurements can be accurate to 0.5%.

Here we describe the drift characteristic of oxygen optodes and show a new approach to use near-surface and in-air O_2 measurements as an in situ calibration reference. At the same time, we want to illustrate the utility of and caveats associated with optode in-air measurements.

2. Methods

a. Drift characteristic

An Aanderaa optode (Aanderaa Data Instruments AS) model 4330 serial number (SN) 564 was multipoint calibrated in the laboratory four times in 3 years using the method described by Bittig et al. (2012). Results from these repeated calibrations are shown in Fig. 1 with calculations being based on coefficients from the initial calibration (April 2011) and the McNeil and D'Asaro

---

∂ Denotes Open Access content.

Corresponding author address: Henry Bittig, Marine Biogeochemistry Department, GEOMAR Helmholtz Centre for Ocean Research Kiel, Düsternbrooker Weg 20, 24105 Kiel, Germany.
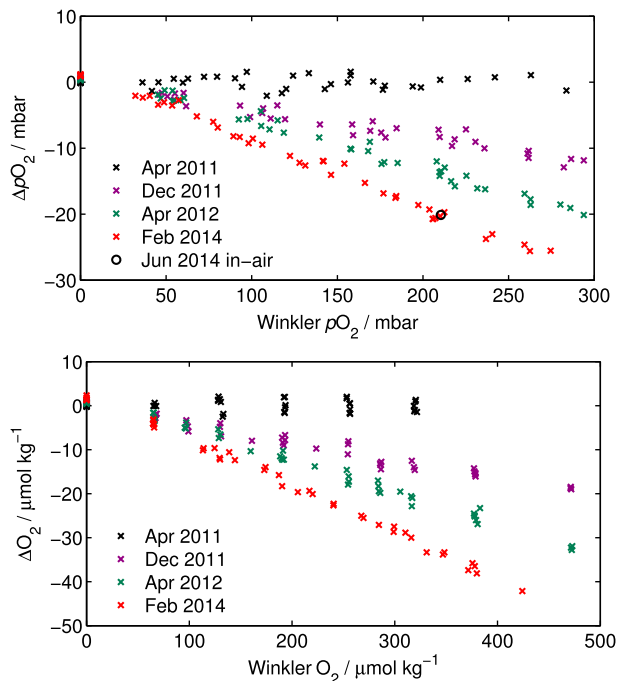E-mail: hbittig@geomar.de

FIG. 1. Drift characteristic of optode 4330 SN 564. The initial calibration [April 2011, black crosses, McNeil and D'Asaro (2014) model] was applied to the sensor data of subsequent calibrations (colored crosses) and the difference to the Winkler reference plotted against the Winkler reference. (top) The data as partial pressure and (bottom) the data as concentration. The predeployment in-air pO_2 measurement on board R/V *Pourquois pas?* is shown as a black circle (see section 3a). The main effect of optode drift is a reduced O_2 sensitivity, i.e., a slope effect. (Note that slopes are identical for pO_2 and O_2 concentration.) A secondary effect is an oxygen-independent offset with a trend toward apparently higher values (see zero values). For details of the April 2011 and December 2011 calibrations, see Fig. 11B in Bittig et al. (2012).

(2014) model. The optode tends to read *lower* with time and the drift shows a linear relation with O_2 (slope < 1, approximately -10% in 3 years). At the same time, there is an O_2-independent offset toward *higher* O_2 (approximately $+2\,\mu mol\,kg^{-1}$ in 3 years). Robust regression parameters are given in Table 1. The drift characteristic is thus dominated by a decrease in the sensor response (slope) superimposed by a small offset that works in the opposite direction.

Oxygen optodes are based on dynamic luminescence quenching, that is, the reduction of luminescence lifetime in the presence of O_2. In principle, quenching follows the Stern–Volmer equation,

$$\frac{\Lambda_0}{\Lambda} = 1 + K_{SV}\,pO_2, \qquad (1)$$

with Λ_0 and Λ being the lifetime in the absence and presence of O_2, respectively, and K_{SV} being the Stern–Volmer constant.

TABLE 1. Comparison of laboratory recalibrations against the April 2011 calibration [with the McNeil and D'Asaro (2014) model]. Robust regression parameters are given for the slope and the intercept (based on pO_2 and O_2 concentration) with CIs at the 95% level.

Calibration	Slope	Intercept (pO_2 mbar^{-1})	Intercept [O_2 ($\mu mol\,kg^{-1}$)$^{-1}$]
Apr 2011	1.000 ± 0.004	-0.1 ± 0.5	$+0.1 \pm 0.8$
Dec 2011	0.957 ± 0.003	$+0.3 \pm 0.4$	$+0.3 \pm 0.6$
Apr 2012	0.929 ± 0.003	$+1.1 \pm 0.5$	$+1.7 \pm 0.6$
Feb 2014	0.898 ± 0.002	$+1.3 \pm 0.3$	$+2.2 \pm 0.5$

The dominant drift pattern (slope < 1) can be attributed to a reduced O_2 sensitivity—that is, a reduced K_{SV}—that could be caused by a degraded O_2 accessibility of the luminophore—for example, due to migration or a decreased O_2 diffusivity inside the sensing membrane—that reduces the quenching frequency. The counteractive positive offset arises from a reduced lifetime Λ_0 of the luminophore itself, which is in line with a potential migration or a change in the immediate luminophore vicinity, for example, a sensing membrane degradation.

In reality, optodes deviate from a linear Stern–Volmer behavior and a number of parametric models exist to relate sensor data (phase shift and temperature) to oxygen (e.g., Aanderaa high-order polynomials; Uchida et al. 2008; McNeil and D'Asaro 2014). While numbers vary somewhat with the choice of the model, the drift characteristic (Fig. 1) is model independent. However, none of today's models strictly follows the physical principles of phase-shift detection oxygen optodes.[1] Consequently, we see no consistent trends in any single or subset of calibration coefficients.

We observed this drift characteristic for recalibrations of other Aanderaa optodes as well and believe it is a generic feature. Based on a limited set of calibrations of Sea-Bird SBE63 optodes (Sea-Bird Electronics, Inc.) in our laboratory and by the manufacturer, the same appears to apply to these sensors. Both Aanderaa and Sea-Bird Electronics optodes use the same luminophore and sensing membrane.

However, we cannot make a quantitative statement about the drift rate due to a limited number of recalibrations. D'Asaro and McNeil (2013) and Tengberg and

---

[1] This includes the McNeil and D'Asaro (2014) model. McNeil and D'Asaro's [2014, their Eq. (6)] basic assumption is that for a two-site approach, individual lifetimes simply add up to the "mean" lifetime detected by phase shift according to their fraction. While this holds for intensities, the case is more complicated for lifetimes and phase-shift detection (Lakowicz 2006, chapter 5).
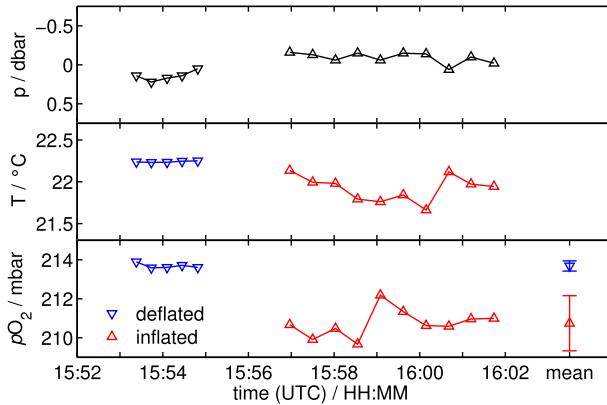
FIG. 2. Near-surface samples of (top) hydrostatic pressure, (middle) optode temperature, and (bottom) optode pO_2 with deflated air bladder (downward triangles, in water) and inflated air bladder (upward triangles, in air) for float F0272 (WMO ID 6900890). Surface waters are supersaturated for cycle 019 and mean deflated and inflated pO_2 are given with $\pm 2\sigma$ error bars.

Hovdenes (2014) indicate that old optodes/sensing membranes (e.g., the Aanderaa optode model 4330F SN 135, see below) drift at a much smaller rate than new ones.

b. Navis dual-O_2 float and near-surface measurement sequence

A Navis float (Sea-Bird Electronics, Inc. SN F0272; WMO 6900890) was equipped with two oxygen optodes, a Sea-Bird SBE63 integrated into the CTD's pumped path and an Aanderaa model 4330 SN 1280 attached to a short stalk (10 cm) on the float's top cap, thereby reaching about midheight of the CTD cage (estimated 20 cm above the sea surface).

In normal float applications, the CTD pump is switched off at 6 dbar (to avoid contamination of the conductivity cell), which is therefore the shallowest SBE63 optode observation.

A special near-surface sequence for the Aanderaa optode was implemented in the Navis float's firmware: At the end of its profile, five samples (20-s intervals) are taken with the air bladder deflated, that is, just below the water–air interface (approximately 0.3 dbar). After that, the air bladder is inflated and 10 samples (30-s intervals) are taken with the optode extending into the air. All data presented here stem from the Aanderaa optode.

A typical example of this near-surface sequence is shown in Fig. 2. Spikes in pressure during inflated sampling indicate that the optode is occasionally submerged/wetted during these "in air" measurements.

The float was deployed on 27 September 2013, near 16°N, 17.6°W in the eastern tropical North Atlantic oxygen minimum zone and stayed about 50–200 nm offshore the West African coast. It was set to a 5-day cycle

interval and surfaced in the afternoon until cycle 44, when the cycle interval was reduced to 4.75 days to have it surface at different times of the day.

c. Predeployment optode calibrations

The Aanderaa optode 4330 SN 1280 was multipoint factory calibrated (accuracy: $2\,\mu\text{mol kg}^{-1}$ or 1.5%; Tengberg and Hovdenes 2014) just 1.5 months prior to the deployment and laboratory multipoint calibrated (RMSE: $1.2\,\mu\text{mol kg}^{-1}$ to triplicate Winkler samples) 2 months prior to the deployment using the method described by Bittig et al. (2012).

d. CTD-O_2 deployment cast and match to float profile

A lightweight sensor package consisting of an SBE37-IMP Microcat (Sea-Bird Electronics, Inc.) and an Aanderaa fast-response optode model 4330F SN 135 attached to a custom logger was lowered to 409 dbar [ca. $+0.5$ $(-0.15\,\text{dbar s}^{-1})^{-1}$] average descent/ascent velocity, 6-s logging intervals) to obtain a reference CTD-O_2 profile just before the float launch and 18 h before completion of the first float profile.

Extensive multipoint laboratory calibrations (following Bittig et al. 2012) of the 4330F optode 2 weeks before as well as 3.5 and 8.5 months after the deployment have a mean bias of $+0.1\,\mu\text{mol kg}^{-1}$ (mean RMSE: $1.5\,\mu\text{mol kg}^{-1}$), indicating that this optode was indeed stable. We therefore have high confidence in the reference profile even in the absence of discrete Winkler samples.

The reference and float profile were matched on a mixed axis x of potential density σ_θ and pressure p. The intention is to have an isopycnal match below the mixed layer depth (to account for isopycnal vertical displacements) and to have an isobaric match above the mixed layer depth (where near-homogeneous density makes an isopycnal match impossible and diel density variations of the surface layer can be accounted for in depth space). For this, pressure is translated into a distortion δ_p in density space as follows:

$$\delta_p = (\Sigma - \sigma_\theta|_{p=0})\frac{\text{MLD} - p}{\text{MLD}}, \quad p \leq \text{MLD} \qquad (2)$$

$$\delta_p = 0\,\text{kg m}^{-3}, \qquad\qquad p > \text{MLD} \qquad (3)$$

where MLD is the pressure of the mixed layer depth. The mixed axis x is then simply the sum of density profile σ_θ and pressure-based distortion δ_p:

$$x = \sigma_\theta + \delta_p. \qquad (4)$$

The term $(\Sigma - \sigma_\theta|_{p=0})$ in Eq. (2) is thus the scaling parameter for pressure within the mixed layer and the parameter Σ determines $x|_{p=0}$. It was (arbitrarily) set to

$10 \, \text{kg m}^{-3}$, so that δ_p dominates over σ_θ variations within the mixed layer.

In addition, mixed layer samples were given a fivefold weight in the regression against the reference to account for the float's bias in the number of surface samples against deeper samples.

e. Air pO_2 calculations

Near-surface float pO_2 was calculated using optode temperature and phase shift and the Uchida et al. (2008) model as described in Bittig et al. (2012).

NCEP–NCAR reanalysis data[2] of atmospheric pressure p_{air}, relative humidity $\varphi^{10\,m}$, and air temperature $T_{air}^{10\,m}$ at 10 m were used to provide an independent atmospheric $pO_{2,air}$ reference. Water vapor pressure p_{vap} was scaled to the optode height (ca. 0.2 m) assuming a logarithmic profile with a roughness length scale of $z_0 = 10^{-4} \, \text{m}$ (Subrahamanyam and Ramachandran 2003) according to

$$p_{vap} = p_{vap}^{*,S} + (\varphi^{10\,m} p_{vap}^{*,10\,m} - p_{vap}^{*,S}) \cdot \frac{\ln(0.2 \, \text{m}/z_0)}{\ln(10 \, \text{m}/z_0)}, \quad (5)$$

where $p_{vap}^{*,S}$ and $p_{vap}^{*,10\,m}$ are the salinity- and temperature-dependent saturation water vapor pressures at the sea surface and at 10 m, respectively (Weiss and Price 1980). The atmospheric $pO_{2,air}$ is then calculated as

$$pO_{2,air} = \chi O_2 (p_{air} - p_{vap}), \quad (6)$$

where $\chi O_2 = 0.209\,46$ is the mixing ratio of O_2 in dry air (Glueckauf 1951).

3. Results and discussion

a. Precision of in-air measurements

Under ideal field conditions, the precision achievable with in-air measurements can be as low as 0.3 mbar (2σ) (Fig. 3). For this test, the above-mentioned Aanderaa optode 4330 SN 564 was mounted on a Bio-Argo float (lovbio059c, PROVOR CTS4, nke Instrumentation; WMO 6901646) and set to sample in air (50-s intervals) on deck (shaded, windward, wetted optode foil) of R/V *Pourquois pas?* just before deployment in the Irminger Sea. While temperature and phase shift vary somewhat, optode pO_2 (based on the laboratory calibration performed 4 months prior) is highly stable.
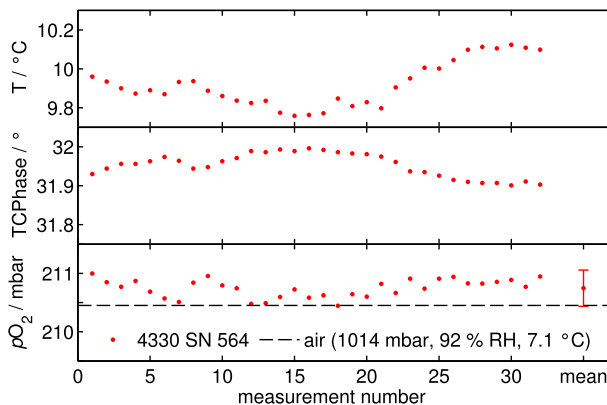
FIG. 3. Optode 4330 SN 564 in-air measurements (50-s interval) on board R/V *Pourquois pas?* before deployment of float lovbio059c (WMO ID 6901646). (top to bottom) Optode temperature, phase shift, and pO_2 (with mean $\pm 2\sigma$). Air pO_2 ($pO_{2,air}$) calculated using Eq. (6) with shipboard meteorological observations is shown as a dashed line for reference.

Using this laboratory calibration, the difference (i.e., accuracy) to an atmospheric pO_2 based on shipboard meteorological observations [Eq. (6)] is +0.3 mbar, indicating that the drift rate for this optode decreased substantially since the first (re)calibration in 2011 (see Fig. 1, top panel).

b. CTD-O_2 deployment cast calibration

Figure 4 shows the first float profile of Navis F0272 together with the deployment cast. Float pO_2 was calculated using the laboratory calibration (green crosses), factory calibration (yellow circles), and a slope- and offset-corrected laboratory calibration (red dots) with the deployment cast as reference (slope: 1.037, offset: +1.4 mbar, RMSE to deployment cast: $6.3 \, \mu\text{mol kg}^{-1}$ including oxycline, mixed layer bias: $+0.2 \, \mu\text{mol kg}^{-1}$).

Both the laboratory and factory calibration suggest an accuracy of $1.2 - 3 \, \mu\text{mol kg}^{-1}$. This is exceeded, however, by offsets in the mixed layer of -8.3 and $-5.1 \, \mu\text{mol kg}^{-1}$, respectively, which follows the previously observed pattern of optodes drifting toward too low sensor readings (e.g., Bittig et al. 2012; Fig. 1). However, a drift of approximately -3.5% in 2 months exceeds the rates previously reported [$\approx -1\%$ (2 months)$^{-1}$; D'Asaro and McNeil 2013] and may be caused by tropical temperatures during shipment and storage.

c. Near-surface measurements

Near-surface F0272 float measurements of pO_2 together with NCEP–NCAR-based air pO_2 are shown in Fig. 5 up to cycle 090. In-water (deflated) measurements agree well with mixed layer data (not shown). However,
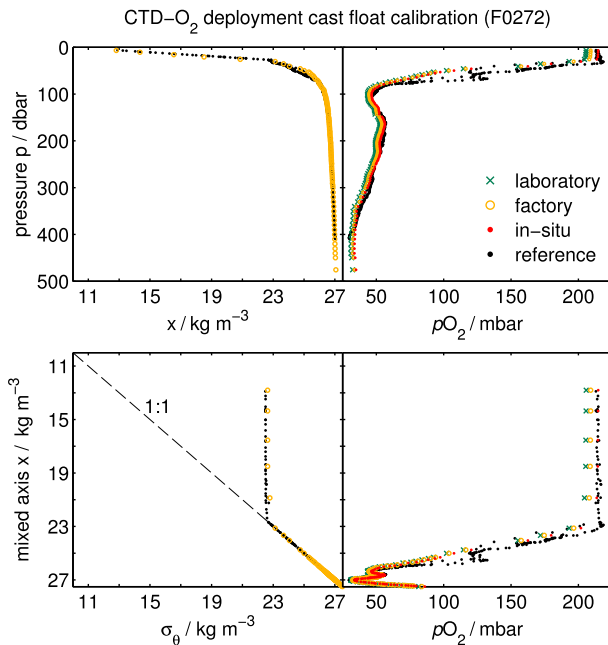
FIG. 4. CTD-O_2 reference cast (black dots) and first F0272 (WMO ID 6900890) float profile (18 h later) of (left) x and σ_θ and (right) pO_2 against (top) pressure and (bottom) the mixed axis x. Below the mixed layer ($\approx$30 dbar), x and σ_θ follow the 1:1 line (dashed), i.e., $\delta_p = 0$. Here pO_2 is based on the laboratory (green crosses), factory (yellow circles), and an in situ deployment cast calibration (red dots).

in-air (inflated) measurements are offset to the air reference depending on the in-water pO_2.

While the optode 4330 extends into the air during (most) inflated measurements, the standard-height stalk seems to be too short to remove the effect of occasional wave-caused submersions, causing a marked carry-over effect. However, the carry-over effect is linear with (water) supersaturation and does not seem to depend on daytime (Fig. 6).

Providing the optode works the same in air and water, there should be no carryover at true 100% O_2 saturation, that is,

$$pO_{2,\text{sat}}^{\text{infl}} = pO_{2,\text{sat}}^{\text{defl}} = pO_{2,\text{air}}. \qquad (7)$$

The linear carryover between inflated (in air) and deflated (in water) observations may thus be parameterized as a linear function of (water) supersaturation,

$$pO_2^{\text{infl}} - pO_{2,\text{air}} = c(pO_2^{\text{defl}} - pO_{2,\text{air}}), \qquad (8)$$

where $pO_{2,\text{air}}$ is calculated according to Eq. (6) and c is the observed carry-over slope (Fig. 6, left).

Equation (8) implies the carryover to be independent of environmental conditions, that is, wind speed or wave height. In fact, we do not see a dependence of c on wind speed, which suggests the parameterization with a constant c to be valid even in calm conditions. An explanation as a simple, wave-related "overwash" effect thus might not give the full picture. We would expect a smaller carry-over effect with a higher attachment (longer stalk) of the optode.

Correcting the observed oxygen with a slope m ($pO_2 = m \, pO_{2,\text{obs}}$) as the dominant drift effect (Fig. 1) affects both sides and Eq. (8) becomes

$$m \, pO_{2,\text{obs}}^{\text{infl}} - pO_{2,\text{air}} = c(m \, pO_{2,\text{obs}}^{\text{defl}} - pO_{2,\text{air}}) \qquad (9)$$

and rearrangement yields

$$pO_{2,\text{obs}}^{\text{infl}} = c \, pO_{2,\text{obs}}^{\text{defl}} + \frac{1-c}{m} pO_{2,\text{air}}, \qquad (10)$$

which can be used for a linear regression.

Using NCEP–NCAR reanalysis meteorological data, the slopes m as given in Table 2 were obtained from Eq. (10). The slope differences between calibrations are consistent with direct regressions between calibrations, indicating that the calculations are robust.

The uncertainty for p_{air} in reanalysis models is on the order of 2 mbar (Smith et al. 2001) or better (van den Besselaar et al. 2011; Clissold 2008). This translates to a relatively small absolute error of 0.2% in m.
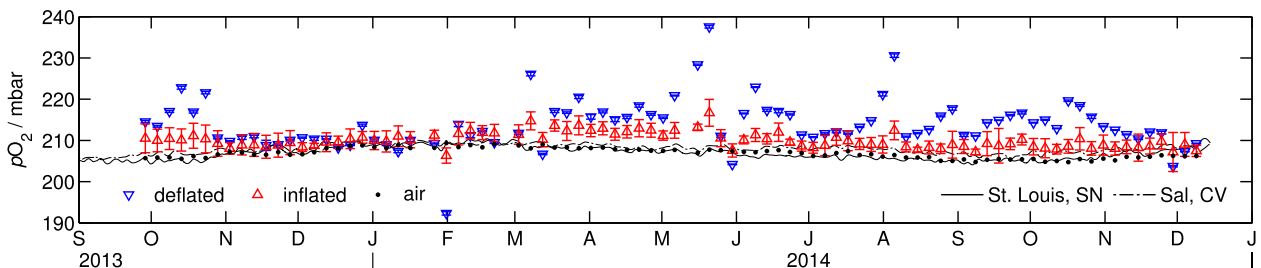

FIG. 5. Time series of near-surface measurements for float F0272 (WMO ID 6900890) using the deployment calibration showing deflated (downward triangles) and inflated (upward triangles) float pO_2 (mean $\pm 2\sigma$). Air pO_2 (dots) as comparison is based on interpolated NCEP–NCAR meteorological data [Eq. (6)]. Black lines give calculated air pO_2 at WMO stations in St. Louis, Senegal (continuous line, station 69600, 100 nm eastward) and on Sal, Cape Verde (dashed–dotted line, station 08594, 250 nm westward).
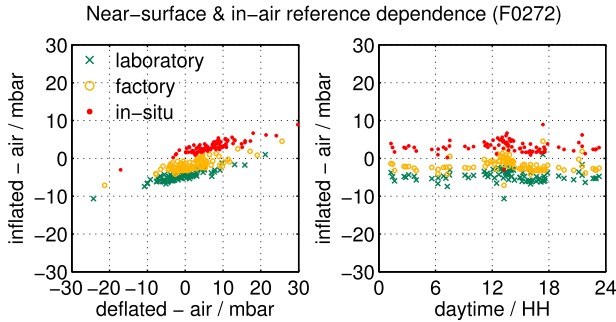
FIG. 6. Plot of float-observed in-air supersaturation (inflated–air) against (left) in-water supersaturation (deflated–air) and (right) daytime for float F0272 (WMO ID 6900890) using the laboratory (green crosses), factory (yellow circles), and in situ calibration (red dots). Error bars are omitted for clarity.

TABLE 2. Correction parameters and fit RMSE of the in-air reference approach for float F0272 using a slope correction [Eq. (10); CI at the 95% level].

Calibration	c	Slope m	RMSE (mbar)
Laboratory	0.22 ± 0.03	1.028 ± 0.001	0.8
Factory	0.21 ± 0.04	1.014 ± 0.002	1.0
In situ	0.22 ± 0.03	0.990 ± 0.001	0.8

The example shown here takes advantage of large surface supersaturations and undersaturations in a coastal upwelling system. Artificially limiting the data to -1% and $+3\%$, respectively, in the saturation anomaly to mimic an oligotrophic open ocean system, the carry-over slope c becomes less constrained but correction slopes m remain unaffected (within confidence intervals).

The influence of the number of near-surface measurements on the in-air reference was estimated by a Monte Carlo approach: A random subset of n near-surface measurements was used for the regression analysis [Eq. (10)] and its slope m compared to the "true" slope m based on all available samples. This was repeated 1000 times for each n and the results are shown in Fig. 7, both for the full record (black) and a record artificially limited to -1% and $+3\%$, respectively, saturation anomaly (red). The correction bias gives the offset in slope m due to the subsetting and the correction uncertainty gives the median confidence interval of m. The analysis shows that subsets are unbiased, that highly precise results can be obtained with a few dozen samples, and that the analysis does not depend on a wide range of saturations—that is, it works in oligotrophic regions as well.

4. Summary

Today's oxygen optodes cannot be used "out of the box" to obtain highly accurate seawater O$_2$ data, so that some kind of in situ reference is required.

Their biggest handicap is a sensitivity drift of significant magnitude (Table 1). However, this drift appears to be systematic and predominantly linear with O$_2$ (Fig. 1). It is thus feasible to correct for such a drift using a proper in situ reference.

An in situ reference profile has the highest yield of information (variety of temperature, oxygen, pressure) and is desirable for a slope and offset correction. However, the reference is limited to the location's hydrography and time of the profile. Moreover, obtaining a profile is complicated if not impossible for opportunistic deployments of autonomous instruments.

In-air measurements as an alternative are accurate, easily implemented, and available for the entire lifetime of the instrument. However, they rely on the air pO_2—that is, a single O$_2$ level—and thus allow only a slope correction.

Nearby meteorological observations (see, e.g., Fiedler et al. 2013), though not likely to be available on many occasions, would be favorable as an atmospheric reference. NCEP–NCAR reanalysis, however, provides global coverage and uncertainty of the model contributes only little to the uncertainty of our analysis. With more recent reanalysis models [e.g., ERA-Interim (Dee et al. 2011), or
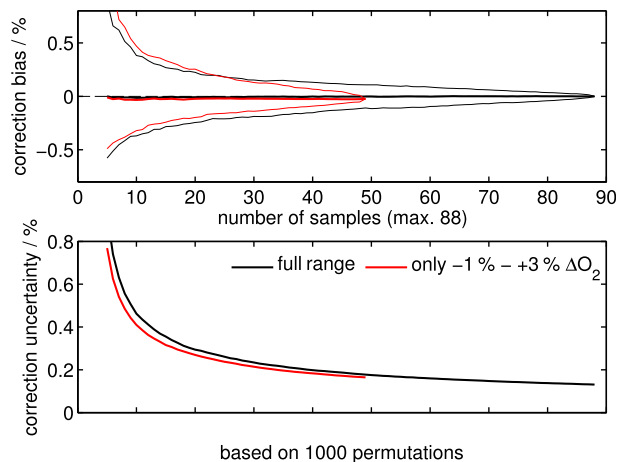

FIG. 7. Monte Carlo analysis for float F0272 (WMO ID 6900890) of the (top) correction bias (offset on slope m compared to complete analysis) and (bottom) uncertainty (confidence of slope m) due to subsetting based on 1000 repetitions each. Thick lines give the median value, while thin lines represent the 2.5% percentile and 97.5% percentile, respectively, i.e., they frame 95% of the data. Results using the full range or a limited $[-1\%; +3\%]$ saturation anomaly range (given in black and red, respectively) do not differ significantly.

MERRA (Rienecker et al. 2011] and future improvements, this uncertainty will diminish further.

Despite the systematic carry-over effect causing a bias in float-observed "in air" pO_2, our approach yields well-determined [0.4-mbar 95% confidence interval (CI)] and consistent results (similar offsets between different calibrations as from a direct comparison). Noise in the data and the magnitude of the carry-over effect (i.e., the slope c) are likely reduced with a higher optode attachment (longer stalk), which would improve the analysis.

Both approaches (in situ and in air) match within 1%, much better than the typical accuracy obtained today (Takeshita et al. 2013). It appears that the in situ deployment calibration of float F0272 is slightly too high (Table 2), but this may just illustrate the accuracy achievable with these methods.

Moreover, a comparison of the first 20 and the 20 most recent in-air measurements indicates that the optode of float F0272 has been stable during the deployment (slope m of 0.992 ± 0.003 vs 0.99 ± 0.003 relative to the in situ calibration).

Our in-air correction approach requires the oxygen optode to be capable of in-air measurements and integration of the near-surface sequence both into the float's firmware and data transmission. Since a reference $pO_{2,air}$ can be derived globally using reanalysis models, this correction is not limited in space or time. Therefore, it might be implemented as a standard quality control routine for the entire Argo-O_2 array (Gruber et al. 2010), significantly improving its data accuracy and coherence.

In conclusion, in-air and near-surface optode measurements have the potential to overcome major limitations of current autonomous O_2 observations: they are technically and logistically feasible (often in contrast to a reference profile), accurate to 1%, available for the entire deployment period, and could be applied universally to the entire O_2 float array.

REFERENCES

Bittig, H. C., B. Fiedler, T. Steinhoff, and A. Körtzinger, 2012: A novel electrochemical calibration setup for oxygen sensors and its use for the stability assessment of Aanderaa optodes. *Limnol. Oceanogr.: Methods,* **10,** 921–933, doi:10.4319/lom.2012.10.921.

Clissold, P., Ed., 2008: Candidate Earth Explorer core missions: A-SCOPE—Advanced space carbon and climate observation of planet Earth. Reports for Assessment, ESA SP-1313/1, 109 pp. [Available online at http://esamultimedia.esa.int/docs/SP1313-1_ASCOPE.pdf.]

D'Asaro, E. A., and C. McNeil, 2013: Calibration and stability of oxygen sensors on autonomous floats. *J. Atmos. Oceanic Technol.,* **30,** 1896–1906, doi:10.1175/JTECH-D-12-00222.1.

Dee, D. P., and Coauthors, 2011: The ERA-Interim reanalysis: Configuration and performance of the data assimilation system. *Quart. J. Roy. Meteor. Soc.,* **137,** 553–597, doi:10.1002/qj.828.

Emerson, S., and S. Bushinsky, 2014: Oxygen concentrations and biological fluxes in the open ocean. *Oceanography,* **27,** 168–171, doi:10.5670/oceanog.2014.20.

Fiedler, B., P. Fietzek, N. Vieira, P. Silva, H. C. Bittig, and A. Körtzinger, 2013: In situ CO_2 and O_2 measurements on a profiling float. *J. Atmos. Oceanic Technol.,* **30,** 112–126, doi:10.1175/JTECH-D-12-00043.1.

Glueckauf, E., 1951: The composition of atmospheric air. *Compendium of Meteorology,* T. F. Malone, Ed., Amer. Meteor. Soc., 3–12.

Gruber, N., and Coauthors, 2010: Adding oxygen to Argo: Developing a global in situ observatory for ocean deoxygenation and biogeochemistry. *Proceedings of Ocean-Obs'09: Sustained Ocean Observations and Information for Society,* J. Hall, D. E. Harrison, and D. Stammer, Eds., Vol. 2, ESA Publ. WPP-306, doi:10.5270/OceanObs09.cwp.39.

Körtzinger, A., J. Schimanski, and U. Send, 2005: High quality oxygen measurements from profiling floats: A promising new technique. *J. Atmos. Oceanic Technol.,* **22,** 302–308, doi:10.1175/JTECH1701.1.

Lakowicz, J. R., Ed., 2006: *Principles of Fluorescence Spectroscopy.* Springer, 954 pp.

McNeil, C. L., and E. A. D'Asaro, 2014: A calibration equation for oxygen optodes based on physical properties of the sensing foil. *Limnol. Oceanogr.: Methods,* **12,** 139–154, doi:10.4319/lom.2014.12.139.

Rienecker, M. M., and Coauthors, 2011: MERRA: NASA's Modern-Era Retrospective Analysis for Research and Applications. *J. Climate,* **24,** 3624–3648, doi:10.1175/JCLI-D-11-00015.1.

Smith, S. R., D. M. Legler, and K. V. Verzone, 2001: Quantifying uncertainties in NCEP reanalyses using high-quality research vessel observations. *J. Climate,* **14,** 4062–4072, doi:10.1175/1520-0442(2001)014<4062:QUINRU>2.0.CO;2.

Subrahamanyam, D. B., and R. Ramachandran, 2003: Wind speed dependence of air-sea exchange parameters over the Indian Ocean during INDOEX, IFP-99. *Ann. Geophys.,* **21,** 1667–1679, doi:10.5194/angeo-21-1667-2003.

Takeshita, Y., T. R. Martz, K. S. Johnson, J. N. Plant, D. Gilbert, S. C. Riser, C. Neill, and B. Tilbrook, 2013: A climatology-based quality control procedure for profiling float oxygen data. *J. Geophys. Res. Oceans,* **118,** 5640–5650, doi:10.1002/jgrc.20399.

Tengberg, A., and J. Hovdenes, 2014: Information on long-term stability and accuracy of Aanderaa oxygen optodes; information about multipoint calibration system and sensor option overview. Aanderaa Data Instruments AS Tech. Note,

14 pp. [Available online at http://www.aanderaa.com/media/pdfs/2014-04-O2-optode-and-calibration.pdf.]

——, and Coauthors, 2006: Evaluation of a lifetime-based optode to measure oxygen in aquatic systems. *Limnol. Oceanogr.: Methods,* **4,** 7–17, doi:10.4319/lom.2006.4.7.

Uchida, H., T. Kawano, I. Kaneko, and M. Fukasawa, 2008: In situ calibration of optode-based oxygen sensors. *J. Atmos. Oceanic Technol.,* **25,** 2271–2281, doi:10.1175/2008JTECHO549.1.

van den Besselaar, E. J. M., M. R. Haylock, G. van der Schrier, and A. M. G. Klein Tank, 2011: A European daily high-resolution observational gridded data set of sea level pressure. *J. Geophys. Res.,* **116,** D11110, doi:10.1029/2010JD015468.

Weiss, R. F., and B. A. Price, 1980: Nitrous oxide solubility in water and seawater. *Mar. Chem.,* **8,** 347–359, doi:10.1016/0304-4203(80)90024-9.